Intelligent Multifunctional $VO_2/SiO_2/TiO_2$ Coatings for Self-Cleaning, Energy-Saving Window Panels

Michael J. Powell[a], Raul Quesada-Cabrera[a]*, Alaric Taylor[b], Diana Teixeira[a], Ioannis Papakonstantinou[b], Robert G. Palgrave[a], Gopinathan Sankar[a], Ivan P. Parkin[a]*.

[a]University College London, Department of Chemistry, Materials Chemistry Centre, 20 Gordon Street, London WC1H 0AJ.
[b]University College London, Department of Electronic and Electrical Engineering, Torrington Place, London WC1E 7JE.
E-mail: *i.p.parkin@ucl.ac.uk; r.quesada@ucl.ac.uk

ABSTRACT: Monoclinic vanadium (IV) oxide (VO_2) has received much attention for applications as intelligent solar control coatings, with the potential to reduce the need for both heating and air conditioning loads within building infrastructure. Chemical vapour deposition –a high-throughput industrially scalable method– is an ideal technology for the deposition of VO_2 thin films on window panels. However, these films suffer from poor adhesion and are chemically susceptible to attack. In addition, the VO_2 films with optimum solar modulation are unfortunately translucent, restraining their commercial use in energy-efficient fenestration. In this work, multi-functional, robust, layered $VO_2/SiO_2/TiO_2$ films were quickly deposited on glass substrates using atmospheric-pressure chemical vapour deposition and fully characterised using structural, vibrational spectroscopy and electron microscopy techniques. The $VO_2/SiO_2/TiO_2$ thin films were designed to exhibit excellent solar modulation properties as well as high transparency and resistance to abrasion, compared to single VO_2 films of the same thickness. The films also showed self-cleaning properties comparable to those of commercial Pilkington Activ™ glass, as demonstrated here during the photodegradation of a model organic pollutant (stearic acid). The SiO_2 acted as a barrier layer, preventing the diffusion of Ti^{4+} ions into the VO_2 layer but it also promoted the optical properties and allowed for superior thermochromic behaviour when compared to single VO_2 films. The system was modelled to determine the effect of the individual components on the properties of the overall material. It was found that the deposition of the SiO_2/TiO_2 overlayer resulted in a dramatic improvement of visible light transmission (~30 % increase when compared to single layer analogues) whilst also doubling the solar modulation of the material.

INTRODUCTION: Managing heat loads in building infrastructure through central heating and air-conditioning has been estimated to produce ~30 % of all anthropogenic greenhouse gas emissions.[1, 2] This has encouraged research into the design and development of energy-efficient approaches in order to reduce the energy required to maintain a comfortable working/living environment. One of the primary routes to achieving this goal would be the development of 'smart' coatings for building fenestration,[3-5] as windows account for the largest energy losses from buildings. The two most widely researched materials as energy-efficient coatings are electrochromic[6, 7] and thermochromic.[5, 8] Thermochromic materials exhibit a temperature-induced switch for the transmission/reflection of long-wave irradiation (heat) and thus do not require any additional energy to function.

Vanadium (IV) oxide (VO_2) is a widely researched material due to its first-order phase transition from a monoclinic to tetragonal (rutile) geometry, which is accompanied by a large optical change in the near IR (the rutile phase is highly reflective of near IR wavelengths).[9, 10] This phase transition also involves changes in electrical conductivity. The monoclinic phase is a semiconductor, with a distinct band-gap (~0.7 eV), and the rutile phase shows semi-metallic properties. These characteristic features make VO_2 a unique material for thermochromic applications.[4, 11, 12] Nevertheless, there are several issues with implementing VO_2 thin films in such applications: (a) the relatively high metal-to-semiconductor transition (MST) temperature (68 °C);[13] (b) the low visible light transmission due to the yellow/brown colour of the films;[14, 15] (c) their poor adherence on glass;[16] and (d) their high susceptibility to chemical attack.[17] The poor visible light transmission is a particular problem for the application of VO_2 for solar control coatings, due to the strong absorption of visible wavelengths owing to the small optical band-gap of VO_2.[18] Methods to improve visible light transmission have included the doping of Mg[19, 20] and F[21, 22] and the deposition of multi-layered films.[4, 23, 24]

Doping VO_2 with appropriate metal ions has been widely reported as an effective approach to tune both the MST temperature and the optical properties of the films in the visible range.[20, 25, 26] The introduction of large cations, such as W, Nb or Mo, into the monoclinic phase is particularly interesting since the MST temperature can be reduced to a practical range (~25 °C).[21, 27, 28] The resulting W,

Nb or Mo-doped films are conveniently blue, which is visually pleasant and suitable for window coatings. Unfortunately, the doping approach has an impact on hysteresis around the transition temperature,[29] which is undesirable, and the doped films are still chemically vulnerable. A convenient approach to overcome this problem is the deposition of a protective transparent coating onto the VO_2 film. This has been achieved by sputtering multilayers of VO_2 and amorphous silica, with higher levels of silica showing an increase in visible transmission whilst maintaining the thermochromism.[30] Calculations have shown that the incorporation of dielectric materials, such as SiO_2, can alter the transmissive properties of the VO_2 thin films increasing visible light transmission.[4, 12, 14]

Some authors have used titanium dioxide (TiO_2) as a protective layer for the VO_2 film,[24, 31, 32] aiming at the development of multifunctional thermochromic/self-cleaning coatings for window applications. The films in these studies were deposited by sputtering, with the VO_2 layer being intercalated between two TiO_2 films, in all cases both photocatalytic and thermochromic behaviour was observed in the deposited films. These films also showed an increase in visible light transmission due to the anti-reflective properties of the TiO_2 overlayer, meaning that more of the incident light was able to pass through the film improving transmission. Atmospheric Pressure Chemical Vapour Deposition (APCVD) allows the high-throughput synthesis of multi-layered films, with facile tailoring of individual layers through the incorporation of dopants and critical control over their physical (crystallinity, thickness, etc.) and chemical (stoichiometry, oxidation state, etc.) properties. The APCVD method is easily scalable and it is currently used, for instance, in the production of self-cleaning glass (Pilkington Activ™, SGG BioClean, PPG SunClean), with sales of >£100 m per annum. Unfortunately, the direct deposition of TiO_2 coatings on VO_2 at high temperature (typically 500 °C) results in diffusion of Ti ions into the VO_2 lattice, which increases the MST temperature of the film.[33] Nevertheless, this issue can be easily resolved by intercalation of an ion-barrier interlayer such as SiO_2. Evans *et al*. have previously demonstrated that a SiO_2 barrier layer can prevent the diffusion of ions into TiO_2 when depositing on steel substrates *via* APCVD.[34] Surprisingly, to the best of our knowledge, multilayer $VO_2/SiO_2/TiO_2$ films have never been developed by CVD methods. These types of multilayered systems have been previously described by modelling.[23, 32, 35] It was found that including SiO_2/TiO_2 layers would allow for the modulation of the incident radiation through the difference in refractive properties between the different media, improving visible light transmission if the correct thicknesses of the layers could be achieved. In the current work, multifunctional transparent $VO_2/SiO_2/TiO_2$ thin films with both thermochromic and self-cleaning properties were produced by APCVD. These films showed significant improvement in visible light transmission compared to that of the original single VO_2 layer and, contrary to the latter, they were mechanically and chemically robust. The $VO_2/SiO_2/TiO_2$ films are archetypal and the synthesis method and conditions presented here allow the direct industrial production of advanced energy-efficient building materials.

2. EXPERIMENTAL

2.1 Chemical precursors: Vanadium tetrachloride (Reagent plus® 99.9 % purity), titanium tetrachloride (Reagent plus® 99.9 % purity), tetraethyl orthosilicate (reagent grade 98 % purity) and ethyl acetate (anhydrous, 99.8 % purity) were purchased from Sigma Aldrich. All chemicals were used without additional chemical treatment. Glass-substrates consisted of a 3.4 mm silica coated barrier glass (50 nm SiO_2 layer) obtained from Pilkington. The glass substrate was 90 x 300 mm. Prior to deposition all substrates were cleaned with acetone, 2-propanol and water and left to air dry. Oxygen-free nitrogen (99.9 % purity) was purchased from BOC and used as the carrier gas for all reactions.

2.2 Synthesis conditions: The APCVD rig has been described elsewhere.[36] The precursors were contained in bubblers under nitrogen (N_2) gas flow, which was used as a carrier gas. The bubblers consisted of stainless steel cylinders with brass jackets and heating bands. All lines were heated using heating tapes (*Electrothermal* 400 W, 230 V). The precursors were mixed in stainless steel mixing chambers. The temperature of all components of the system was controlled by k-type thermocouples with *Thermotron* controllers.

In the synthesis of $VO_2/SiO_2/TiO_2$ films, vanadium tetrachloride (VCl_4), titanium tetrachloride ($TiCl_4$), tetraethyl orthosilicate (TEOS, $SiC_8H_{20}O_4$) and ethyl acetate ($C_4H_8O_4$) were used as V, Ti, Si and O sources, respectively. The reactor temperature was set to 550 °C. The plain N_2 gas flow set to 20 L min^{-1} and the plain flow lines heated to 200 °C. The mixing chambers were set to 150 °C. The sample description and respective synthesis conditions of the films discussed in this work are summarised in Table 1. For the deposition of VO_2, the VCl_4 bubbler was set to 80 °C and had a N_2 gas flow set at 0.7 L min^{-1}. The $C_4H_8O_4$ bubbler was set to 40 °C and had a N_2 gas flow set at 0.2 L min^{-1}. In the case of SiO_2, the $SiC_8H_{20}O_4$ bubbler was set to 130 °C with a N_2 gas flow set to 0.7 L min^{-1}. The latter precursor reacted with $C_4H_8O_4$ under the same temperature/flow conditions used in the VO_2 case. For the deposition of TiO_2, the $TiCl_4$ bubbler was set to 75 °C with a N_2 gas flow of 0.6 L min^{-1}; the ethyl acetate was maintained at 40 °C with the N_2 gas flow increased to 0.6 L min^{-1}. The depositions ranged from 1 to 7 minutes in length. After every reaction, the substrates were allowed to cool under nitrogen flow and were only removed from the reaction chamber when the temperature was below 90 °C. Single-layer and multilayer films have been termed here as V–1, V–3 (only VO_2 layer) and VST–1, VST–3 ($VO_2/SiO_2/TiO_2$) in reference to the deposition time of the VO_2 layer (1 and 3 min, respectively).

2.3 Characterisation Methods: X-ray diffraction (XRD) studies were carried out using a Bruker-Axs D8 (GADDS) diffractometer. The instrument operates with a Cu X-ray

source, monochromated ($K\alpha_1$ and $K\alpha_2$) and a 2D area X-ray detector with a resolution of 0.01º (glancing incident angle, θ= 0.3º). The diffraction patterns obtained were compared with database standards from the Inorganic Crystal Structure Database (ICSD), Karlsruhe, Germany. Atomic Force Microscopy scans were made of the VO_2 and TiO_2 samples using a Nanosurf Easyscan 2 system fitted with a Bruker NCLR cantilever. Non-contact tapping mode was used to build a topological map of each samples over an 8x8um area with a lateral resolution of 15nm. Scanning electron microscopy (SEM) was carried out using a Jeol JSM-6700F and secondary electron image on a Hitachi S-3400N field emission instruments (20 KV) and the Oxford software INCA. X-Ray photoelectron spectroscopy (XPS) was performed using a Thermo Scientific K-alpha spectrometer with monochromated Al Kα radiation, a dual beam charge compensation system and constant pass energy of 50 eV (spot size 400 μm). Survey scans were collected in the range 0–1200 eV.

2.4 Functional testing: The thermochromic properties of the samples were studied via absorption UV/vis spectroscopy, using a Perkin Elmer Lambda 950 UV/Vis/NIR Spectrophotometer. The transmission/reflectance spectra were recorded directly on the as-deposited films, which were clamped against the integrating sphere in perpendicular position to the beam path. The samples were gently heated *in situ* using an aluminium high-temperature cell controlled by RS cartridge heaters, Eurotherm temperature controllers and k-type thermocouples. A *Labsphere* reflectance standard was used as reference in the UV/vis measurements. Contact angle measurements were made using a FTA1000 system. A 6.8 μl drop of deionised water was dispensed by gravity from a gauge 30 needle and photographed side on when in-situ on the surface of the sample thin films. The contact angle of the water droplet and the surface is measured by the software from this image. The self-cleaning properties of the coatings were investigated during photocatalytic degradation of stearic acid. A layer of stearic acid was dip-coated onto the films from a chloroform solution (0.05 M). The degradation of the acid was monitored by infrared spectroscopy using a *Perkin Elmer RX-I* spectrometer. The samples were irradiated in a home-built light box equipped with six blacklight blue fluorescent tubes (UVA 6×18 W) and an extractor fan. The irradiance (4 ± 0.2 mW cm^{-2}) at sample position was measured using a *UVX* radiometer (*UVP*). The area of the sample under illumination was 3.14 cm^2.

3. RESULTS AND DISCUSSION:

3.1 Physical properties of the films: The deposition of $VO_2/SiO_2/TiO_2$ was carried out in a single run on glass substrates at 550 °C, as described above (*vide supra*). The robustness of the films was checked by the Scotch-tape test.[37] The single-layer VO_2 films were easily delaminated by this test and they could also be easily removed by rubbing with a piece of cloth. In contrast, the multilayer $VO_2/SiO_2/TiO_2$ films showed strong adherence to the glass substrates and were even resistant to scratching by a steel scalpel. All films were indefinitely stable in air over a period of several months and no pinhole defects were observed.

The single VO_2 layers were unequivocally matched to monoclinic VO_2 by X-ray diffraction (XRD) (**Figure 1**). No trace of impurity phases was observed in these studies. It was interesting to notice that the structural properties of the TiO_2 layer in the multilayered systems were dependent of thickness of the SiO_2 layer. The growth of TiO_2 on a thin SiO_2 layer (sample VST–1, deposition time 1 min) resulted in pure rutile phase, whilst thicker SiO_2 layers (sample VST–1, deposition time 3 min) induced formation of both anatase and rutile structures during deposition of the TiO_2 layer (**Figure 1**(b)). This suggests that the SiO_2 layer initially displays the same lattice parameters as the underlying VO_2 layer, with increasing deposition length causing a shift towards a less pronounced lattice match. Also noticeable was the shifting of anatase and rutile peaks in the XRD data, which indicates the presence of lattice strain caused by the underlying VO_2 phase and the lattice mismatch between the monoclinic VO_2 and rutile (tetragonal) TiO_2 phases.[38] This strain effect is still evident in the thicker SiO_2 deposition (sample VST–3) (Figure 1(b)).

The individual VO_2 films showed a very rough surface, as evidenced by atomic force microscopy (AFM) (**Figure 2**(a)). This was further supported by side on SEM images (**Figure 3**(b)) and water contact angle measurements, where prior to UV irradiation, the VO_2 films showed superhydrophilic (below 5°) contact angles. In contrast, the multilayered $VO_2/SiO_2/TiO_2$ films showed significantly reduced surface roughness in the AFM images (**Figure 2**(b)). This was also evident in the side on SEM images (**Figure 3**(f)) and water contact angles, in these cases were ~70° prior to irradiation. Upon UV irradiation, the multi-layered films showed photo-induced superhydrophilicity as expected for TiO_2.[39] The morphology of the films was assessed by scanning electron microscopy (SEM) (**Figure 3**(a)), with particle shapes ranging from needles to plate-like structures. The needle like structures were also evident in the AFM images for the VO_2 single layer films (**Figure 2**(a)). The multi-layered $VO_2/SiO_2/TiO_2$ showed a more uniform morphology of the top TiO_2 layer (**Figure 3**(b)). The particles are pyramidal in shape in the latter case. This morphology was also evident in the AFM images for the multi-layered films (**Figure 2**(b)). This type of morphology has been previously observed for rutile TiO_2 thin films from CVD processes.[40, 41] There is also a large difference between the size of the VO_2 and TiO_2 particles present in the films, with the VO_2 particles being significantly larger. The SiO_2 layer (**Figure 3**(c)) shows a highly porous film, with column-like structure evident. The pores in the SiO_2 film are on the scale of 1000 ±50 nm. Side-on SEM images allowed an estimation of the thickness of the different layers (**Figure 3**(d)). The VO_2 layer in direct contact with the glass substrate was very uniform in appearance and about 300 ±10 nm in thickness (the sample shown in **Figure 3**(d) is VST-1). This layer is followed by a thicker layer, at-

tributed to SiO_2 (1500 ±50 nm) that shows a series of repeating column-like structures which is in agreement with those seen for the SiO_2 layer (**Figure 3**(c)), interspersed with what appear to be voids again confirming the porous nature of the SiO_2 film. Finally, a third layer at the surface of the film was attributed to TiO_2 and it was approx. 100 nm in thickness. The side-on SEM images also helped to elucidate the reason for the increase in film adhesion on the inclusion of the SiO_2/TiO_2 overlayer. The SiO_2 layer is seen to infill the VO_2 layer, creating points where the SiO_2 layer will be 'anchored' to the underlying SiO_2 barrier layer. This is coupled with a substantial decrease in grain size at the surface, which is known to improve mechanical properties of thin films.[42]

The oxidation environments and the relative percentage of each element (Ti, Si and V) throughout the films were estimated by X-ray photoelectron spectroscopy (XPS). Each individual element had its oxidation state probed, with the Ti, Si and V peaks (Figure 3) at binding energies of 485.7, 103.3 and 515.6 eV, respectively. These binding energies are consistent with Ti^{4+}, Si^{4+} and V^{4+} in their corresponding oxides, namely TiO_2,[43] SiO_2[44] and VO_2,[45] respectively. Depth profiling determined that the surface was Ti rich, with the presence of Si also near the surface, as expected from the highly structured SiO_2 layer, and a weak V signal appearing towards the end of the etching (Figure 3).

3.2 Thermochromic and optical properties: Variable temperature transmission UV/Vis spectroscopy was used in order to determine the thermochromic and optical properties of the films **(Figure 5)**. In all cases, the MST transition temperature was observed c.a. 68 °C, consistent with undoped VO_2 thin films.[5] There was also no difference observed in hysteresis behaviour between the single and multi-layered samples, all sample showed a hysteresis of 5 ±2 °C. It can be clearly seen that the inclusion of the SiO_2 and TiO_2 coatings improved the visible light transmission (T_{lum}) of the films, with an increase of *ca*. 30 and 15 % for samples VST–1 and VST–3, respectively, compared to the equivalent single VO_2 films. Likewise, the thermochromic responses of both multilayered systems were larger than either of the single layered analogues. Reflectance UV/Vis spectra, **Figure 6**, confirmed that the films became more reflective in the near IR when heated beyond the MST. Again, the multi-layered films displayed improved reflectance in the near IR when compared with the single layer analogues, with sample VST-1 (Figure 5 (a)) displaying twice roughly twice in reflectance as large a switch as sample V-1.

To give a more quantitative value to the solar modulation (T_{sol}) and visible light transmission (T_{lum}) of the films, weighted solar modulation and visible light transmission values were obtained from the UV/Vis spectra **(Table 2)**. The calculations used to determine T_{sol} and T_{lum} followed a procedure described in a previous publication.[46] The improvement in visible light transmission of the multilayered samples (VST–1 and VST–3) was accompanied by a substantial improvement in total solar modulation (ΔT_{sol}), which roughly doubled that of the corresponding single VO_2 layers (samples V–1 and V–3, respectively). The best performing film in terms of solar modulation was sample VST–3, which showed a total of 15.29 % (ΔT_{sol}) (Table 2). This value is very close to the maximum possible solar modulation for VO_2 thin films (~17 %).[46]

Calculations of the transmittance spectra through the multilayer structures were performed using a transfer matrix method. The refractive index of TiO_2, SiO_2 and VO_2 were taken from Devore,[47] Palik[48] and Mlyuka,[23] respectively. Our model assumed the multilayer film stack was deposited upon a glass (SiO_2) substrate and irradiated from a broadband light source in air. The reported transmittance values were taken between the region of air directly in contact with the TiO_2 layer and the region of glass in direct contact with the bottom VO_2 layer. The SiO_2 layer in our system is optically thicker than the coherence length of broadband sunlight. Therefore, we expect a broad phase distribution at the SiO_2-VO_2 interface for light that has passed fully through the SiO_2 layer. This effectively inhibits the formation of a resonant cavity within the SiO_2 layer, decoupling resonance between the TiO_2 and VO_2 layers. In order to model incoherence in the SiO_2 layer, we adapted our transfer matrix calculation method. Both electric field and phase information were maintained within the TiO_2 and VO_2 layers (and at their respective boundaries). However, within the SiO_2 layer only electric field information was preserved. The effect of including our incoherence modification can be seen in the difference between **Figure 7**(a) (coherent) and **Figure 7(b)** (incoherent). Coherence within the SiO_2 would lead to resonant peaks in the transmittance spectra which were not observed in our UV/Vis measurements (**Figure 5**).

Our initial model for the VST-1 multilayer stack consisted of a 100-nm TiO_2 layer, a 1300-nm SiO_2 layer and a 300-nm VO_2 layer and was based upon SEM images of the film (**Figure 3**). However, our transfer matrix transmittance calculations did not match the UV/Vis measurements of VST-1 (**Figure 7(b)** and **Figure 4(a)**). In order to investigate whether the mismatch between our calculations and the experimental data was a result of non-uniform film thickness, we performed a series of calculations in which every combination of film thicknesses (within given bounds) contributed toward an average transmittance. The spectra for sample VST-1 (uniform thickness, **Figure 7(b)**) can be compared with the average spectra for the same multilayer film with an induced uncertainty (**Figure 7(c)**), i.e. 100 ± 10nm TiO_2 layer, a 1300 ± 50 nm SiO_2 layer and a 300 ± 10 nm VO_2 layer. The contribution of uncertainty averaging did not account for the difference in transmittance between the experimental results for sample VST-1 and our transfer matrix calculations. Therefore, we performed a study in which the thickness of our VO_2 layer was varied between 0 and 300 nm. The smart window metrics, T_{lum} and ΔT_{sol}, were calculated for each thickness of VO_2 and can be seen in Figure 7(a). It was found that the experimentally determined smart window metrics for sample VST-1 were most closely represented by a transfer matrix model in which the VO_2

thickness was modified to become 50 nm (**Figure 8(b)**). This may suggest that the VO_2 film produced during our APCVD method may have had a low density.

Other researchers have proposed methods for increasing the visible light transmission of VO_2 thin films. These methods have included Mg^{2+} doping,[18] depositing thin films (below 50 nm) of VO_2,[49] $TiO_2/VO_2/TiO_2/VO_2/TiO_2$ multi-layered 'sandwich structures[23] and using anti-reflection layers.[4] These methods will be explored in future work using the APCVD set-up detailed in this paper.

3.3 Self-cleaning properties: The multilayered $VO_2/SiO_2/TiO_2$ films displayed water contact angles of 70–90°, which are typical for TiO_2 thin films.[50] UV irradiation contributes to increase hydrophilicity of TiO_2 surfaces to <10°. This shows that the films still exhibit photo-induced superhydrophilicity which is a key property for self-cleaning coatings.[51] The self-cleaning properties of these films were studied during photocatalytic degradation of octadecanoic (stearic) acid. This fatty acid is considered a model organic pollutant, which typically deposits on window panels, tiles and other surfaces. The photo-degradation of stearic acid is also convenient from a kinetic point of view (the reaction follows zero order kinetics and thus the rate is independent of the initial concentration of the acid) and it can be easily monitored using infrared spectroscopy (FTIR). These IR-active bands correspond to C–H stretching modes. The total area under these peaks was used to evaluate the degradation of the acid upon UVA irradiation (4 mW cm^{-2}) (**Figure 9**(a)). The degradation rates were estimated from the initial 30–40 % decrease of the initial amount of acid. It could be inferred from Figure 8(a) that sample VST–1 showed negligible activity whilst the degradation rate corresponding to sample VST–3 was comparable to that of a standard Pilkington Activ™ glass. The latter is a commercially available self-cleaning glass, which contains a thin TiO_2 layer (~15 nm) deposited by CVD methods.[52]

The photocatalytic results can be conveniently expressed in terms of formal quantum efficiency (ξ), given as molecules of acid degraded per incident photon (units, molec $photon^{-1}$). The molecules degraded are estimated directly from the degradation rates using a conversion factor (1 $cm^{-1} \equiv 9.7\times10^{15}$ molec cm^{-2}) from the literature.[53] It could be confirmed (Figure 8(b)) that the ξ values of both VST–3 and Pilkington Activ™ samples were comparable and even slightly higher for the former, whilst sample VST–1 had virtually no activity in the degradation of the acid. The latter observation was expected since the TiO_2 layer in sample VST–1 was a pure rutile phase, which is known to be inactive in the photo-oxidation of organic pollutants.

4. CONCLUSIONS: The simple production of multilayered $VO_2/SiO_2/TiO_2$ films has been demonstrated by atmospheric-pressure chemical vapour deposition. The synthesis of these systems is directly scalable for industrial use and it offers a great advantage towards the development of advanced multifunctional coatings for energy-efficient, intelligent window applications. The use of a SiO_2/TiO_2 protective bilayer prevents any potential chemical attack and improved the mechanical properties of the coating, making the film more adherent and robust. The presence of TiO_2 on the surface resulted in self-cleaning properties (photoactivity and photo-induced superhydrophilicity) comparable to those demonstrated for commercially available self-cleaning glass.

Furthermore, the SiO_2/TiO_2 overlayer dramatically increased the visible light transmission as well as improving the solar modulation of the original VO_2 film. The best performing multilayered film produced in this work showed a solar modulation value (15.29 %) which is very close to the maximum possible solar modulation for VO_2 thin films. The experimental values of both visible light transmission and solar modulation were compared to smart window metrics obtained after transfer matrix transmittance calculations. In terms of visible light transmission, it was concluded that our experimental results were only expected for significantly thinner VO_2 films, whilst preserving maximum solar modulation.

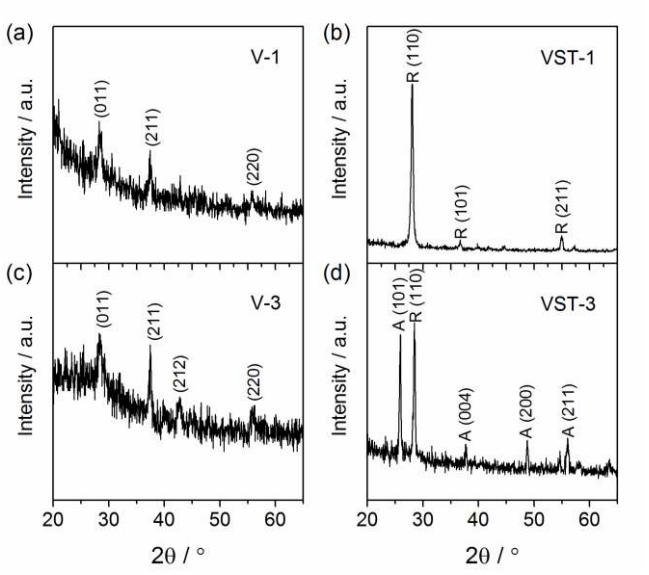

Figure 1. XRD patterns of (a-c) single-layer monoclinic VO_2 films (samples V-1 and V-3, respectively) and (b-c) multilayer $VO_2/SiO_2/TiO_2$ films (samples VST-1 and VST-3, respectively). The latter patterns correspond to TiO_2 polymorphs (anatase and rutile peaks indicated as A and R, respectively) and the diffraction peaks are shifted due to lattice strain from the underlying VO_2/SiO_2 layers.

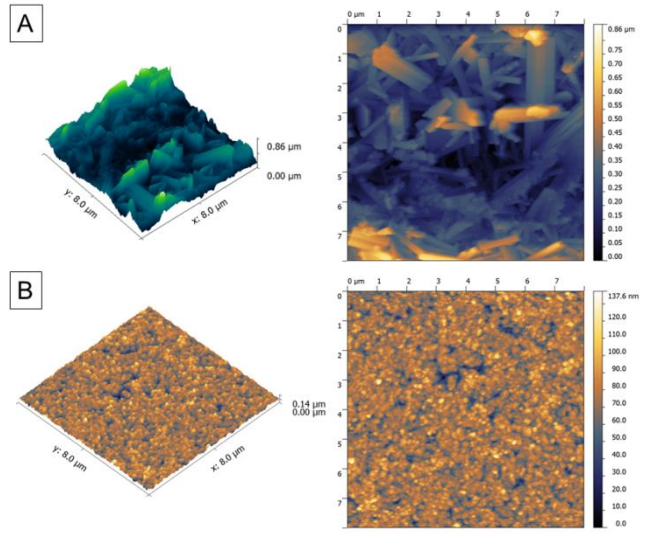

Figure 2: Atomic force microscopy images for (a) a typical VO_2 coating, showing needle like structures and high surface roughness; (b) a typical TiO_2 surface coating for a multilayered $VO_2/SiO_2/TiO_2$ film, showing significant reduction in surface roughness compared with the VO_2 analogue.

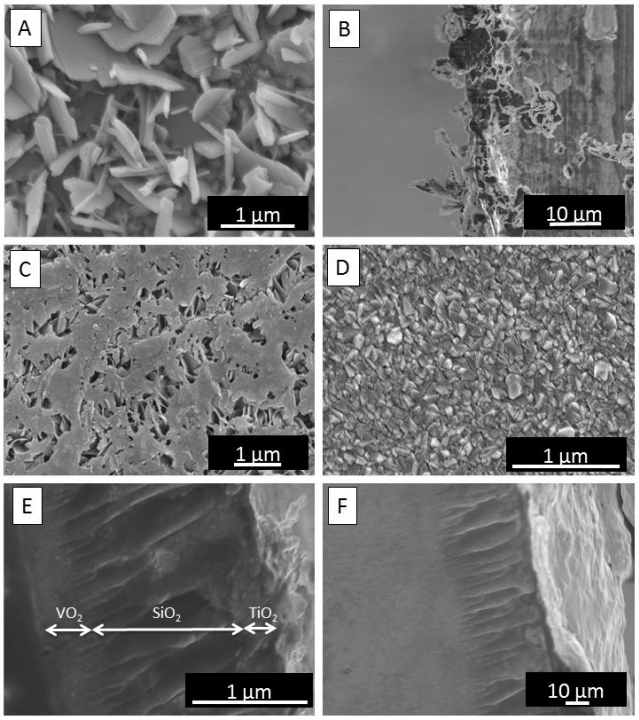

Figure 3. SEM images for (a) a typical VO_2 coating, showing both needle and plate-like structures; (b) side-on SEM image showing typical surface features for VO_2 single layer; (c) porous structure of the SiO_2 interlayer, as deposited on a VO_2 coating; (d) typical surface morphology of the TiO_2 layer in the $VO_2/SiO_2/TiO_2$ system; (e) side-on SEM image of a $VO_2/SiO_2/TiO_2$ film (sample VST-1). Labels included for clarity; (f) side-on SEM showing typical surface features for multilayered $VO_2/SiO_2/TiO_2$ film.

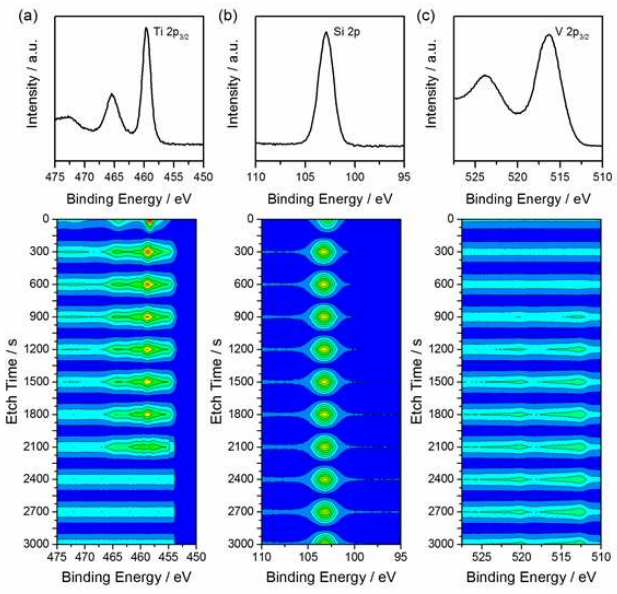

Figure 4. XPS spectra of (a) Ti $2p_{3/2}$ peaks in the Ti^{4+} environment; (b) Si 2p peak in the Si^{4+} environment; (c) V $2p_{3/2}$ peaks in the V^{4+} environment. Depth profile data is included as a contour map, illustrating the change in intensity of the Ti, Si and V environments upon etching time.

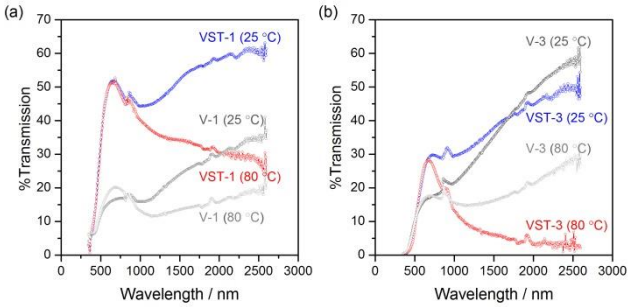

Figure 5. Variable temperature transmission UV/Vis spectra of single VO_2 and multi-layered $VO_2/SiO_2/TiO_2$ systems (samples V-*t* and VST-*t*, with VO_2 and SiO_2 deposition time *t* = 1 or 3 min), as indicated, at 25 and 80 °C.

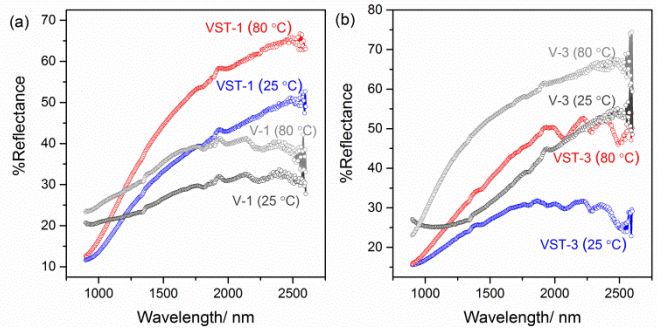

Figure 6. Variable temperature reflectance UV/Vis spectra of single and multi-layered $VO_2/SiO_2/TiO_2$ systems (samples V-*t* and VST-*t*, with VO_2 and SiO_2 deposition time *t* = 1 or 3 min), as indicated, at 25 and 80 °C.

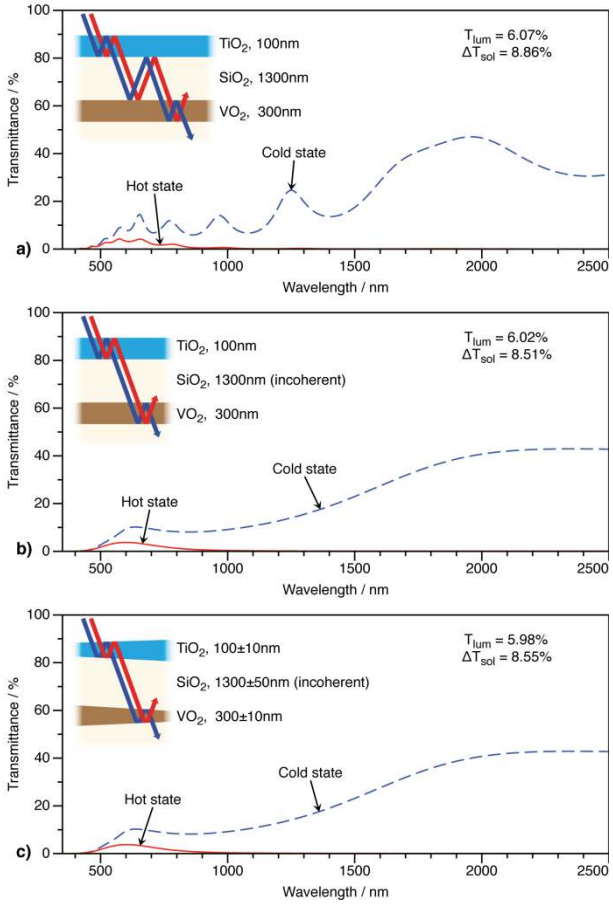

Figure 7. Calculated transmittance spectra of a $VO_2/SiO_2/TiO_2$ system assuming (a) coherent conditions and uniform thickness of layers; (b) incoherent conditions and uniform thickness of layers and (c) incoherent conditions and non-uniform thickness of layers.

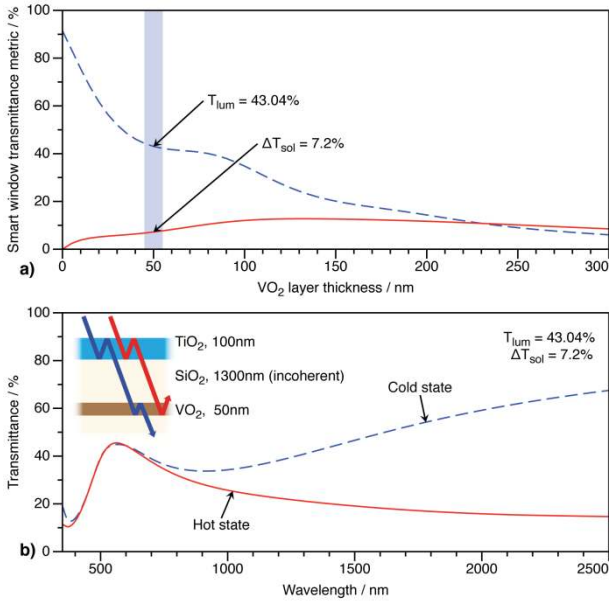

Figure 8. (a) Calculated visible transmission (T_{lum}) and solar modulation (ΔT_{sol}) for a range of thicknesses of VO_2 films giving a value of 50 nm for the properties observed in sample VST-1 and (b) calculated thermochromic response for sample with 50 nm VO_2 film.

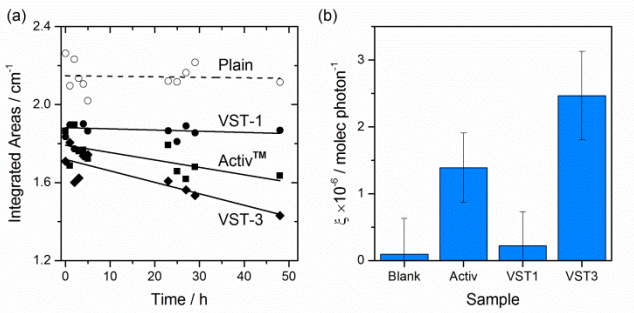

Figure 9. Photocatalytic degradation of stearic acid on multilayered $VO_2/SiO_2/TiO_2$ systems (samples VST-1 and VST-3) compared with Pilkington Activ™ glass. (a) Integrated areas of stearic acid during UVA illumination (I= 4 mW cm^{-2}) and (b) corresponding formal quantum efficiencies (ξ). The values obtained on plain glass, in the absence of a coating, are included for reference.

Table 1. Sample description and synthesis conditions of the films studied in this work, given as bubbler temperature (*T*, °C) and gas flow rate (*F*, L min^{-1}). *t* indicates the deposition time for each layer (1 or 3 min), except for the TiO_2 layer which was always 1 min.

#	Sample	Layer	Precursor	T (°C)	F (L min^{-1})
V–*t*	VO_2	VO_2	VCl_4	80	0.7
			$C_4H_8O_4$	40	0.2
VST–*t*	$VO_2/SiO_2/TiO_2$	VO_2	VCl_4	80	0.7
			$C_4H_8O_4$	40	0.2
		SiO_2	$SiC_8H_{20}O_4$	130	0.7
			$C_4H_8O_4$	40	0.2
		TiO_2	$TiCl_4$	75	0.6
			$C_4H_8O_4$	40	0.6

Table 2. Corresponding weighted solar modulation (T_{sol}), weighted visible light transmission (T_{lum}) and total solar modulation (ΔT_{sol}) values for single and multilayered films. All values are represented as percentages (%).

	Thickness	Hot state		Cold state		
	(nm)	T_{sol}	T_{lum}	T_{sol}	T_{lum}	ΔT_{sol}
V-1	~300	15.19	16.55	18.33	14.15	3.14
V-3	~1000	15.83	14.08	23.91	13.60	8.09
VST-1	~1800	38.56	44.19	46.19	44.24	7.63
VST-3	~5000	13.55	18.23	28.83	17.81	15.29

AUTHOR INFORMATION

Corresponding Author

*University College London, Department of Chemistry, Materials Chemistry Centre, 20 Gordon Street, London WC1H 0AJ.

Author Contributions

The manuscript was written through contributions of all authors.

ACKNOWLEDGMENT

This work was funded by EPSRC, ICE Glazing Project (EP/M003353/1).

REFERENCES

1. Buildings, U.-S.; Initiative, C., Buildings and climate change: status, challenges and opportunities. In Paris: United Nations Environment Programme: 2007.
2. Omer, A. M., Energy use and environmental impacts: a general review. *J. Renewable Sustainable Energy* **2009,** 1, 053101/1-053101/29.
3. Warwick, M. E.; Binions, R., Advances in thermochromic vanadium dioxide films. *Journal of Materials Chemistry A* **2014,** 2, 3275-3292.
4. Granqvist, C. G.; Lansaker, P. C.; Mlyuka, N. R.; Niklasson, G. A.; Avendano, E., Progress in chromogenics: New results for electrochromic and thermochromic materials and devices. *Sol. Energy Mater. Sol. Cells* **2009,** 93, 2032-2039.
5. Parkin, I. P.; Binions, R.; Piccirillo, C.; Blackman, C. S.; Manning, T. D., Thermochromic coatings for intelligent architectural glazing. *Journal of Nano research* **2008,** 2, 1-20.
6. Gillaspie, D. T.; Tenent, R. C.; Dillon, A. C., Metal-oxide films for electrochromic applications: present technology and future directions. *J. Mater. Chem.* **2010,** 20, 9585-9592.
7. Granqvist, C. G., Electrochromic devices. *J. Eur. Ceram. Soc.* **2005,** 25, 2907-2912.
8. Granqvist, C. G., Transparent conductors as solar energy materials: A panoramic review. *Sol. Energy Mater. Sol. Cells* **2007,** 91, 1529-1598.
9. Goodenough, J. B., Anomalous properties of the vanadium oxides. *Annu. Rev. Mater. Sci.* **1971,** 1101-38.
10. Zylbersztejn, A.; Mott, N. F., Metal-insulator transition in vanadium dioxide. *Phys. Rev. B* **1975,** 11, 4383-95.
11. Manning, T. D.; Parkin, I. P.; Pemble, M. E.; Sheel, D.; Vernardou, D., Intelligent Window Coatings: Atmospheric Pressure Chemical Vapor Deposition of Tungsten-Doped Vanadium Dioxide. *Chem. Mater.* **2004,** 16, 744-749.
12. Li, S. Y.; Niklasson, G. A.; Granqvist, C. G., Thermochromic fenestration with VO2-based materials: Three challenges and how they can be met. *Thin Solid Films* **2012,** 520, 3823-3828.
13. Goodenough, J. B., Two components of the crystallographic transition in vanadium dioxide. *Journal of Solid State Chemistry* **1971,** 3, 490-500.
14. Li, S. Y.; Niklasson, G. A.; Granqvist, C. G., Nanothermochromics: calculations for VO2 nanoparticles in dielectric hosts show much improved luminous transmittance and solar energy transmittance modulation. *J. Appl. Phys.* **2010,** 108, 063525/1-063525/8.
15. Li, S. Y.; Niklasson, G. A.; Granqvist, C. G., Thermochromics and nanothermochromics: new options for energy efficient fenestration. *Annu. Tech. Conf. Proc. - Soc. Vac. Coaters* **2011,** 54th, 29-34.

16. Binions, R.; Blackman, C. S.; Carmalt, C. J.; O'Neill, S. A.; Parkin, I. P.; Molloy, K.; Apostilco, L., Tin phosphide coatings from the atmospheric pressure chemical vapour deposition of SnX 4 (X= Cl or Br) and PR x H 3– x (R= Cyc hex or phenyl). *Polyhedron* **2002,** 21, 1943-1947.

17. Greenwood, N. N.; Earnshaw, A., *Chemistry of the Elements*. Elsevier: 2012.

18. Li, S.-Y.; Mlyuka, N. R.; Primetzhofer, D.; Hallén, A.; Possnert, G.; Niklasson, G. A.; Granqvist, C. G., Bandgap widening in thermochromic Mg-doped VO2 thin films: Quantitative data based on optical absorption. *Applied physics letters* **2013,** 103, (16), 161907.

19. Mlyuka, N.; Niklasson, G.; Granqvist, C.-G., Mg doping of thermochromic VO2 films enhances the optical transmittance and decreases the metal-insulator transition temperature. *Applied physics letters* **2009,** 95, 171909.

20. Zhou, J.; Gao, Y.; Liu, X.; Chen, Z.; Dai, L.; Cao, C.; Luo, H.; Kanahira, M.; Sun, C.; Yan, L., Mg-doped VO2 nanoparticles: hydrothermal synthesis, enhanced visible transmittance and decreased metal-insulator transition temperature. *Phys. Chem. Chem. Phys.* **2013,** 15, 7505-7511.

21. Burkhardt, W.; Christmann, T.; Meyer, B. K.; Niessner, W.; Schalch, D.; Scharmann, A., W- and F-doped VO2 films studied by photoelectron spectrometry. *Thin Solid Films* **1999,** 345, 229-235.

22. Kiri, P.; Warwick, M. E. A.; Ridley, I.; Binions, R., Fluorine doped vanadium dioxide thin films for smart windows. *Thin Solid Films* **2011,** 520, 1363-1366.

23. Mlyuka, N. R.; Niklasson, G. A.; Granqvist, C. G., Thermochromic VO2-based multilayer films with enhanced luminous transmittance and solar modulation. *Phys. Status Solidi A* **2009,** 206, 2155-2160.

24. Takahashi, M.; Tsukigi, K.; Dorjpalam, E.; Tokuda, Y.; Yoko, T., Effective photogeneration in TiO2/VO2/TiO2 multilayer film electrodes prepared by a sputtering method. *The Journal of Physical Chemistry B* **2003,** 107, 13455-13458.

25. Manning, T. D.; Parkin, I. P., Atmospheric pressure chemical vapour deposition of tungsten doped vanadium(iv) oxide from VOCl3, water and WCl6. *J. Mater. Chem.* **2004,** 14, 2554-2559.

26. Piccirillo, C.; Binions, R.; Parkin, I. P., Nb-doped VO2 thin films prepared by aerosol-assisted chemical vapour deposition. *Eur. J. Inorg. Chem.* **2007**, 4050-4055.

27. Blackman, C. S.; Piccirillo, C.; Binions, R.; Parkin, I. P., Atmospheric pressure chemical vapour deposition of thermochromic tungsten doped vanadium dioxide thin films for use in architectural glazing. *Thin Solid Films* **2009,** 517, 4565-4570.

28. Batista, C.; Carneiro, J.; Ribeiro, R. M.; Teixeira, V., Reactive pulsed-DC sputtered Nb-doped VO2 coatings for smart thermochromic windows with active solar control. *J. Nanosci. Nanotechnol.* **2011,** 11, 9042-9045.

29. Xu, Y.; Huang, W.; Shi, Q.; Zhang, Y.; Song, L.; Zhang, Y., Synthesis and properties of Mo and W ions co-doped porous nano-structured VO2 films by sol–gel process. *Journal of Sol-Gel Science and Technology* **2012,** 64, 493-499.

30. Kakiuchida, H.; Jin, P.; Tazawa, M., Control of Optical Performance in Infrared Region for Vanadium Dioxide Films Layered by Amorphous Silicon. *International Journal of Thermophysics* **2010,** 31, 1964-1971.

31. Tang, Z.; Sun, F.; Han, B.; Yu, K.; Zhu, Z.; Chu, J., Tuning Interlayer Exchange Coupling of Co-Doped TiO 2/VO 2 Multilayers via Metal-Insulator Transition. *Physical Review Letters* **2013,** 111, 107203.

32. Jin, P.; Xu, G.; Tazawa, M.; Yoshimura, K., Design, formation and characterization of a novel multifunctional window with VO2 and TiO2 coatings. *Applied Physics A* **2003,** 77, 455-459.

33. Beteille, F.; Morineau, R.; Livage, J.; Nagano, M., Switching properties of V 1– x Ti x O 2 thin films deposited from alkoxides. *Materials Research Bulletin* **1997,** 32, 1109-1117.

34. Evans, P.; Sheel, D. W., Photoactive and antibacterial TiO2 thin films on stainless steel. *Surf. Coat. Technol.* **2007,** 201, 9319-9324.

35. Li, S.-Y.; Niklasson, G. A.; Granqvist, C.-G., Nanothermochromics with VO2-based core-shell structures: Calculated luminous and solar optical properties. *Journal of Applied Physics* **2011,** 109, 113515.

36. Wilkinson, M.; Kafizas, A.; Bawaked, S. M.; Obaid, A. Y.; Al-Thabaiti, S. A.; Basahel, S. N.; Carmalt, C. J.; Parkin, I. P., Combinatorial Atmospheric Pressure Chemical Vapor Deposition of Graded TiO2-VO2 Mixed-Phase Composites and Their Dual Functional Property as Self-Cleaning and Photochromic Window Coatings. *ACS Comb. Sci.* **2013,** 15, 309-319.

37. Griffith, J.; Qiu, Y.; Tombrello, T., Ion-beam-enhanced adhesion in the electronic stopping region. *Nuclear Instruments and Methods in Physics Research* **1982,** 198, 607-609.

38. Muraoka, Y.; Hiroi, Z., Metal-insulator transition of VO2 thin films grown on TiO2 (001) and (110) substrates. *Applied physics letters* **2002,** 80, 583-585.

39. Takeuchi, M.; Sakamoto, K.; Martra, G.; Coluccia, S.; Anpo, M., Mechanism of photoinduced superhydrophilicity on the TiO2 photocatalyst surface. *The Journal of Physical Chemistry B* **2005,** 109, 15422-15428.

40. Evans, P.; Pemble, M. E.; Sheel, D. W., Precursor-directed control of crystalline type in atmospheric pressure CVD growth of TiO2 on stainless steel. *Chemistry of Materials* **2006,** 18, 5750-5755.

41. Hyett, G.; Green, M.; Parkin, I. P., X-ray diffraction area mapping of preferred orientation and phase change in TiO2 thin films deposited by chemical vapor deposition. *Journal of the American Chemical Society* **2006,** 128, 12147-12155.

42. Thompson, C. V.; Carel, R., Stress and grain growth in thin films. *Journal of the Mechanics and Physics of Solids* **1996,** 44, 657-673.

43. Diebold, U.; Madey, T., TiO2 by XPS. *Surface Science Spectra* **1996,** 4, 227-231.

44. Shibata, H.; Kimura, S.; Takatoh, H., Deposition of SiO2 Thin Films by Combined Low-Energy Ion-Beam and Molecular-Beam Epitaxial Method. *Japanese Journal of Applied Physics* **2000,** 39, 1327.

45. Silversmit, G.; Depla, D.; Poelman, H.; Marin, G. B.; De Gryse, R., Determination of the V2p XPS binding energies for different vanadium oxidation states (V 5+ to V 0+). *Journal of Electron Spectroscopy and Related Phenomena* **2004,** 135, 167-175.

46. Taylor, A.; Parkin, I.; Noor, N.; Tummeltshammer, C.; Brown, M. S.; Papakonstantinou, I., A bioinspired solution for spectrally selective thermochromic VO2 coated intelligent glazing. *Optics Express* **2013,** 21, A750-A764.

47. DeVore, J. R., Refractive indices of rutile and sphalerite. *JOSA* **1951,** 41, 416-417.

48. Palik, E. D., *Handbook of optical constants of solids*. Academic press: 1998; Vol. 3.

49. Kang, L.; Gao, Y.; Luo, H., A novel solution process for the synthesis of VO2 thin films with excellent thermochromic properties. *Acs Applied Materials & Interfaces* **2009,** 1, 2211-2218.

50. Mills, A.; Elliott, N.; Hill, G.; Fallis, D.; Durrant, J. R.; Willis, R. L., Preparation and characterisation of novel thick sol-gel titania film photocatalysts. *Photochemical & Photobiological Sciences* **2003,** 2, 591-596.

51. Parkin, I. P.; Palgrave, R. G., Self-cleaning coatings. *Journal of Materials Chemistry* **2005,** 15, 1689-1695.

52. Mills, A.; Lepre, A.; Elliott, N.; Bhopal, S.; Parkin, I. P.; O'Neill, S. A., Characterisation of the photocatalyst Pilkington

Activ (TM): a reference film photocatalyst? *Journal of Photochemistry and Photobiology a-Chemistry* **2003,** 160, 213-224.

53. Mills, A.; Wang, J. S., Simultaneous monitoring of the destruction of stearic acid and generation of carbon dioxide by self-cleaning semiconductor photocatalytic films. *Journal of Photochemistry and Photobiology a-Chemistry* **2006,** 182, 181-186.

Table of Contents Graphic